arXiv:1402.3865v2 [cond-mat.quant-gas] 30 May 2014

Static structure factors for a spin-1 Bose-Einstein condensate

L. M. Symes, D. Baillie, and P. B. Blakie
Jack Dodd Centre for Quantum Technology, Department of Physics, University of Otago, Dunedin, New Zealand

We consider the total density and spin density fluctuations of a uniform spin-1 Bose-Einstein condensate within the Bogoliubov formalism. We present results for the total density and spin density static structure factors for all four magnetic phases. A key result of our work is a set of analytic predictions for the structure factors in the large and small momentum limits. These results will be useful in current experiments aiming to develop a better understanding of the excitations and fluctuations of spinor condensates.

I. INTRODUCTION

A spinor Bose-Einstein condensate (BEC) consists of atoms with a spin degree of freedom [1, 2]. In addition to exhibiting spatial coherence, a spinor condensate also displays a range of spin orders, determined by the interactions and externally applied magnetic field. Various aspects of the phase diagram and condensate dynamics have been explored in experiments, particularly for the case of spin-1 where the atoms can access three magnetic sublevels (e.g. see [3–11]). An important feature of this system is that it exhibits a rich excitation spectrum with phonon and magnon branches [1, 2, 12, 13].

In this paper we develop a formalism to describe the fluctuations of the various densities of interest for a spin-1 condensate. Our primary focus is the total number density and the components of the spin density, motivated by the capability to measure these quantities directly in experiments (e.g. by Stern-Gerlach [14–17] and dispersive [8, 11, 18–20] probing). We characterise these fluctuations by calculating the relevant static structure factors. The Bogoliubov description of the spin-1 condensate is expected to provide a good description of the system for temperatures well below the condensation temperature. Within this framework, we present both numerical results and analytic expressions for the limiting behavior of the static structure factors. For each of the four distinct magnetic phases of the spin-1 condensate, we relate how the three Bogoliubov excitation branches contribute to the fluctuations. Of particular interest are the antiferromagnetic and broken-axisymmetric phases, in which a second continuous symmetry associated with the spin degree of freedom is broken [in addition to the $U(1)$ gauge symmetry]. This is revealed by the emergence of a second Nambu-Goldstone mode [21].

For the case of the total density, the long wavelength limit of the structure factor is $k_B T/Mc_n^2$ where T is the temperature, M is the atomic mass and c_n is the speed of sound (also see [21]). This is equivalent to the thermodynamic result $\Delta N^2 = Vn^2 k_B T\kappa$, where ΔN^2 is the number variance in a volume V of a system of average density n with isothermal compressibility $\kappa = 1/nMc_n^2$. We also analyse the structure factors for the three components of spin density. Analogous to the relation between fluctuations and compressibility for the density static structure factor, the long wavelength limit of the spin density structure factors reveals the magnetic susceptibility of the condensate.

While the dynamic and static structure factors are well characterised for the case of scalar condensates (e.g. see [22]), much less work has been done on multicomponent systems, although we note theoretical studies of binary condensates [23, 24] and an approximate treatment of the finite temperature transverse spin-density correlations in a quasi-two-dimensional ferromagnetic condensate (see Appendix B of Ref. [25]). Experimentally the static structure factor can be determined directly from fluctuation measurements (e.g. see [26, 27]), off-resonant light scattering [28] and Bragg spectroscopy [29, 30]. Notably, in recent experiments spin-dependent Bragg spectroscopy has been used to measure the z-spin density of a spin-$\frac{1}{2}$ Fermi gas [31], and speckle imaging has been employed to measure the compressibility and magnetic susceptibility of a strongly interacting Fermi gas [32]. Along this path a number of experiments with spin-1 condensates have made fluctuation measurements, particularly in application to dynamical regimes (e.g. [9, 14, 33]) and spin-squeezing [16]. We also note a recent proposal to use magnetic spectroscopy to impart energy to a spinor condensate for the purposes of probing its excitation spectrum [34].

The structure of this paper is as follows. In Sec. II we introduce the Hamiltonian and meanfield description of the spin-1 system. We present the phase diagram and briefly discuss the four distinct equilibrium phases. In Sec. III we present a general treatment of fluctuations in the spin-1 system by introducing a generalised two-point density correlation function, from which we obtain the static structure factors. In Sec. IV we discuss the excitation spectrum and the relationship of each branch of the spectrum to the fluctuations of interest for each of the four equilibrium phases. We present both numerical and analytic results for the various static structure factors. The analytic results are summarised in Table II. Finally, we conclude our work in Sec. V, discussing the possible applications of our results.

II. SYSTEM

A. Hamiltonian

We consider a uniform three-dimensional spin-1 Bose gas subject to a uniform magnetic field along z. The single-particle description of the atoms is provided by the Hamiltonian

$$(h_0)_{ij} = \left[-\frac{\hbar^2\nabla^2}{2M} - pi + qi^2\right]\delta_{ij}, \tag{1}$$

where p and q are the coefficients of the linear[1] and quadratic Zeeman terms, respectively, and the subscripts $i, j = \{-, 0, +\}$ refer to the $m_F = \{-1, 0, 1\}$ magnetic sublevels of the atoms. The value of q is tunable independently of p (e.g. see [35, 36]) and can be both positive and negative.

The cold-atom Hamiltonian, including interactions, is given by [1, 2]

$$\hat{H} = \int d\mathbf{x}\, \hat{\boldsymbol{\psi}}^\dagger(\mathbf{x}) h_0 \hat{\boldsymbol{\psi}}(\mathbf{x}) + :\frac{c_0}{2}\hat{n}(\mathbf{x})\hat{n}(\mathbf{x}) + \frac{c_1}{2}\hat{\mathbf{f}}(\mathbf{x})\cdot\hat{\mathbf{f}}(\mathbf{x}):, \tag{2}$$

where :: indicates normal ordering, $\hat{\boldsymbol{\psi}} = [\hat{\psi}_+, \hat{\psi}_0, \hat{\psi}_-]^T$ is the spinor boson field operator, and the superscript T indicates the transpose operation. The interaction terms involve the total density $\hat{n}$ and the spin density $\hat{\mathbf{f}} = [\hat{f}_x, \hat{f}_y, \hat{f}_z]^T$ given by

$$\hat{n}(\mathbf{x}) = \hat{\boldsymbol{\psi}}^\dagger(\mathbf{x})\hat{\boldsymbol{\psi}}(\mathbf{x}), \tag{3}$$

$$\hat{f}_\alpha(\mathbf{x}) = \hat{\boldsymbol{\psi}}^\dagger(\mathbf{x})\mathrm{F}_\alpha\hat{\boldsymbol{\psi}}(\mathbf{x}), \quad \alpha = x, y, z, \tag{4}$$

where $\{\mathrm{F}_\alpha\}$ are the spin-1 matrices. The parameters c_0 and c_1 are the density and spin dependent interaction parameters, respectively, and are given by $c_0 = 4\pi\hbar^2(a_0 + 2a_2)/3M$ and $c_1 = 4\pi\hbar^2(a_2 - a_0)/3M$, with a_S ($S = 0, 2$) being the s-wave scattering length for the scattering channel of total spin S.

B. Meanfield description of system

Here we shall be interested in temperatures well below the condensation temperature, where the field can be written as

$$\hat{\boldsymbol{\psi}}(\mathbf{x}) = \sqrt{n}\,\boldsymbol{\xi} + \hat{\boldsymbol{\delta}}(\mathbf{x}), \tag{5}$$

where $\langle\hat{\boldsymbol{\psi}}\rangle = \sqrt{n}\,\boldsymbol{\xi}$ is the (uniform) condensate field, $n = N/V$ is the condensate density, V is the volume, N is the number of condensate atoms, and $\boldsymbol{\xi} = [\xi_+, \xi_0, \xi_-]^T$ is the normalized condensate spinor. The operator $\hat{\boldsymbol{\delta}} = [\hat{\delta}_+, \hat{\delta}_0, \hat{\delta}_-]^T$ represents the non-condensate field.

1. *Condensate and phase diagram*

The condensate is obtained as the lowest energy solution of the Gross-Pitaevskii equation

$$\mu\boldsymbol{\xi} = \left[h_0 + c_0 n\mathbb{1} + c_1\sum_\alpha f_\alpha \mathrm{F}_\alpha\right]\boldsymbol{\xi}, \tag{6}$$

where $\mathbb{1}$ is the 3×3 identity matrix and

$$f_\alpha = n\boldsymbol{\xi}^\dagger \mathrm{F}_\alpha \boldsymbol{\xi}, \tag{7}$$

[1] The quantity p also serves as a Lagrange multiplier to constrain the z component of magnetization.

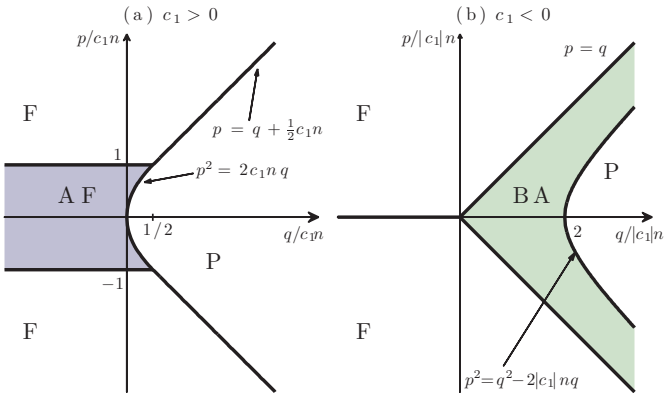

Figure 1. The zero temperature phase diagram of a spin-1 Bose gas for cases with (a) *antiferromagnetic* interactions (i.e. $c_1 > 0$), and (b) *ferromagnetic* interactions (i.e. $c_1 < 0$). The vertical and horizontal axes are the linear and quadratic Zeeman energies (see text) in units of $|c_1|n$, where n is the condensate number density. The phases shown are (F) ferromagnetic, (P) polar, (AF) antiferromagnetic, and broken-axisymmetric (BA) (see Refs. [3, 12]). The rotational symmetry about the direction of the applied field is spontaneously broken in the AF and BA phases.

is the α-component of the condensate spin density. A variety of ground state phases emerge from the competition between the spin-dependent interaction (i.e. $c_1 n$) and the external magnetic field (i.e. p and q). For spin-1 there are four distinct phases distinguished by their magnetization, both along the direction of the external field (i.e. f_z) and perpendicular to it (i.e. $f_\perp \equiv \sqrt{f_x^2 + f_y^2}$). These properties are summarized in Table I, and the parameter regions where each phase is the predicted ground state is shown in Fig. 1.

Phase	Properties
Ferromagnetic (F)	Fully magnetized $\lvert f_z\rvert = n$, $\lvert f_\perp\rvert = 0$. $\boldsymbol{\xi} = [1, 0, 0]^T$ or $[0, 0, 1]^T$.
Polar (P)	Unmagnetized $\lvert f_z\rvert = \lvert f_\perp\rvert = 0$. $\boldsymbol{\xi} = [0, 1, 0]^T$
Anti-ferromagnetic (AF)	Partially magnetized $\lvert f_z\rvert \le n$, $\lvert f_\perp\rvert = 0$. Condensate spinor has non-zero components in the $m_F = \pm 1$ sublevels.
Broken-axisymmetric (BA)	Partially magnetized, but tilts to the z axis giving $f_\perp > 0$. Condensate spinor has non-zero components in all sublevels.

Table I. The phases of a spin-1 BEC, as presented in Fig. 1, categorised according to their magnetization.

Detailed derivations of the ground states and the phase diagram are too lengthy to present here, and we refer the reader to the excellent summary given in Sec. 3.3 of Ref. [12]. We also note here that, in addition to the spin density, an important characterization of the condensate order is provided by

the nematic tensor

$$q_{\alpha\beta} = n\boldsymbol{\xi}^\dagger \mathrm{Q}_{\alpha\beta}\boldsymbol{\xi}, \tag{8}$$

where $\mathrm{Q}_{\alpha\beta} = \frac{1}{2}\left(\mathrm{F}_\alpha\mathrm{F}_\beta + \mathrm{F}_\beta\mathrm{F}_\alpha\right)$ is a 3×3 matrix for each pair of $\alpha, \beta \in \{x, y, z\}$.

2. *Bogoliubov excitations*

The excitations of the condensate are determined by the non-condensate operator. Within a Bogoliubov treatment this operator can be expressed as

$$\hat{\boldsymbol{\delta}}(\mathbf{x}) = \sum_{\mathbf{k}\neq\mathbf{0},\nu} \left(\mathbf{u}_{\mathbf{k}\nu}\hat{\alpha}_{\mathbf{k}\nu} - \mathbf{v}^*_{\mathbf{k}\nu}\hat{\alpha}^\dagger_{-\mathbf{k}\nu}\right)\frac{e^{i\mathbf{k}\cdot\mathbf{x}}}{\sqrt{V}}, \tag{9}$$

where $\{\mathbf{u}_{\mathbf{k}\nu}, \mathbf{v}_{\mathbf{k}\nu}\}$ are the quasiparticle amplitudes, with respective energies $E_{\mathbf{k}\nu}$, and $\nu = \{0, 1, 2\}$ is the spin mode label distinguishing the three solution branches. The quasiparticle operators $\hat{\alpha}_{\mathbf{k}\nu}$ satisfy bosonic commutation relations.

Quite a broad understanding of the quasiparticle solutions has been developed for the spin-1 condensate, however the full review of this is too lengthy to be included here, and we refer the reader to Refs. [12, 21, 37]. We make use of a number of these results in the expressions we derive here for the static structure factors. The results which we present are obtained by diagonalising a 6×6 matrix to determine the quasiparticle energies and amplitudes for the three branches (e.g. see Secs. 5.1 and 5.2 of Ref. [12]). This is done for each k for the numerical results and analytically for the results in Table II.

III. FLUCTUATIONS

A. Observable

Our interest lies in the fluctuations that occur in the total and spin densities of the system, as characterized by the observables given in Eqs. (3) and (4). We generically represent these observables as

$$\hat{w}(\mathbf{x}) = \hat{\boldsymbol{\psi}}^\dagger(\mathbf{x})\mathrm{W}\hat{\boldsymbol{\psi}}(\mathbf{x}), \tag{10}$$

where W is a 3×3 matrix.[2] In the low-temperature regime of interest the mean value is determined by the condensate and is spatially constant, i.e.

$$w = \langle\hat{w}(\mathbf{x})\rangle = n\boldsymbol{\xi}^\dagger\mathrm{W}\boldsymbol{\xi}, \tag{11}$$

and in what follows we consider the fluctuations about this mean value.

[2] In this paper we consider the cases of $\mathrm{W} \in \{\mathbb{1}, \mathrm{F}_x, \mathrm{F}_y, \mathrm{F}_z\}$, i.e. $\hat{w}(\mathbf{x})$ being the total density or a component of the spin density.

B. w density-density correlation function

The spatial fluctuations of $\hat{w}$ are characterized by the two-point correlation function

$$C_w(\mathbf{x} - \mathbf{x}') = \langle\delta\hat{w}(\mathbf{x})\delta\hat{w}(\mathbf{x}')\rangle\,, \tag{12}$$

where we have introduced the fluctuation operator

$$\delta\hat{w}(\mathbf{x}) = \hat{w}(\mathbf{x}) - w. \tag{13}$$

Because we consider a uniform system, C_w only depends on the relative separation of the two points.

It is convenient to rewrite the correlation function in the form

$$C_w(\mathbf{x} - \mathbf{x}') = \langle: \delta\hat{w}(\mathbf{x})\delta\hat{w}(\mathbf{x}') :\rangle + \overline{w^2}\,\delta(\mathbf{x} - \mathbf{x}'), \tag{14}$$

where

$$\overline{w^2} \equiv \langle\hat{\boldsymbol{\psi}}^\dagger(\mathbf{x})\mathrm{W}^2\hat{\boldsymbol{\psi}}(\mathbf{x})\rangle = n\boldsymbol{\xi}^\dagger\mathrm{W}^2\boldsymbol{\xi}. \tag{15}$$

The delta-function term in Eq. (14) represents the autocorrelation of individual atoms (shot noise), and a completely uncorrelated system is one in which $C_w(\mathbf{r}) = \overline{w^2}\,\delta(\mathbf{r})$. The normally ordered term in Eq. (14) thus represents the correlations arising from quantum degeneracy and interaction effects.

C. Static structure factor

The w static structure factor is defined as

$$S_w(\mathbf{k}) \equiv \frac{1}{N}\int d\mathbf{x}\, d\mathbf{x}'\, C_w(\mathbf{x} - \mathbf{x}')e^{-i\mathbf{k}(\mathbf{x}-\mathbf{x}')}, \tag{16}$$

$$= \frac{\langle\delta\hat{w}_{\mathbf{k}}\delta\hat{w}_{-\mathbf{k}}\rangle}{N}. \tag{17}$$

Here $\delta\hat{w}_{\mathbf{k}}$ is the Fourier transformed fluctuation operator

$$\delta\hat{w}_{\mathbf{k}} \equiv \int d\mathbf{x}\, e^{-i\mathbf{k}\cdot\mathbf{x}}\delta\hat{w}(\mathbf{x}), \tag{18}$$

$$\approx \sqrt{N}\sum_\nu \left(\delta\tilde{w}_{\mathbf{k}\nu}\hat{\alpha}_{\mathbf{k}\nu} + \delta\tilde{w}^*_{\mathbf{k}\nu}\hat{\alpha}^\dagger_{-\mathbf{k}\nu}\right), \tag{19}$$

where

$$\delta\tilde{w}_{\mathbf{k}\nu} \equiv \boldsymbol{\xi}^\dagger\mathrm{W}\mathbf{u}_{\mathbf{k}\nu} - \mathbf{v}^T_{\mathbf{k}\nu}\mathrm{W}\boldsymbol{\xi}, \tag{20}$$

is a quantity we refer to as the w fluctuation amplitude. In obtaining Eq. (19) we have neglected higher order terms in the quasiparticle operators, which should be a good approximation at low temperatures.

The static structure factor is then given by

$$S_w(\mathbf{k}) = \sum_\nu |\delta\tilde{w}_{\mathbf{k}\nu}|^2 \coth\left(\frac{E_{\mathbf{k}\nu}}{2k_BT}\right), \tag{21}$$

where we have used that

$$\langle\hat{\alpha}^\dagger{}_{\mathbf{k}\nu}\hat{\alpha}_{\mathbf{k}'\nu'}\rangle = \frac{\delta_{\mathbf{k}\mathbf{k}'}\delta_{\nu\nu'}}{e^{E_{\mathbf{k}\nu}/k_BT} - 1}, \tag{22}$$

with δ_{ab} the Kronecker delta.

In the high k limit, where the kinetic energy is large compared to the thermal and interaction energies, only the uncorrelated part of C_w contributes, and from Eq. (16) we have

$$S_w(k \to \infty) = \frac{1}{n}\overline{w^2}. \tag{23}$$

We refer to this as the uncorrelated limit of the structure factor.

IV. SPECTRA AND STRUCTURE FACTORS

In this section we consider the excitations for the phases shown in Fig. 1, and how they manifest in the various structure factors. To do this we specialise the general discussion of the previous section to the case of total and spin density fluctuations, adopting the notation

$$\hat{w} \to \{\hat{n}, \hat{f}_x, \hat{f}_y, \hat{f}_z\}, \tag{24a}$$
$$\mathrm{W} \to \{\mathbb{1}, \mathrm{F}_x, \mathrm{F}_y, \mathrm{F}_z\}, \tag{24b}$$
$$\delta\tilde{w}_{\mathbf{k}\nu} \to \{\delta\tilde{n}_{\mathbf{k}\nu}, \delta\tilde{f}_{x,\mathbf{k}\nu}, \delta\tilde{f}_{y,\mathbf{k}\nu}, \delta\tilde{f}_{z,\mathbf{k}\nu}\}, \tag{24c}$$
$$S_w(\mathbf{k}) \to \{S_n(\mathbf{k}), S_x(\mathbf{k}), S_y(\mathbf{k}), S_z(\mathbf{k})\}. \tag{24d}$$

In the next subsections we discuss the various phases and their excitation spectra and fluctuations. A key set of results of our research is the analytic expressions for $S_w(\mathbf{k})$ in the $k \to 0$ and $k \to \infty$ limits, for all four phases. These results are listed systematically in Table II and have been validated against numerical calculations. We do not present details of the lengthy derivations here.

For the most commonly realised spinor condensates of ^{87}Rb and ^{23}Na atoms, the spin dependent interaction is much smaller than the spin independent interaction (see Table 2 of Ref. [12]). Additionally ^{23}Na has $c_1 > 0$ (i.e. antiferromagnetic interactions), while ^{87}Rb has $c_1 < 0$ (i.e. ferromagnetic interactions). Here we choose to present results using $c_0 = -250c_1$ for BA, within the range of experimental predictions for ^{87}Rb and using $c_0 = 50c_1$ for other phases, within the range of experimental predictions for ^{23}Na [12]. We adopt the spin healing length,[3] $\xi_s = \hbar/\sqrt{M|c_1|n}$ as a convenient length scale, noting that for our choice of parameters it is a factor of $\sqrt{50}$ or $\sqrt{250}$ larger than the density healing length $\xi_n = \hbar/\sqrt{Mc_0n}$.

A. F phase

1. *Condensate and excitation spectrum*

The F phase occurs for both $c_1 > 0$ and $c_1 < 0$, and in this phase the condensate is completely magnetized in the $m_F = 1$ or -1 states depending on the value of p [see Fig. 1(a), (b)]. We focus on the case $p > 0$ with atoms in the $m_F = 1$ state,

$$\boldsymbol{\xi}^{\mathrm{F}} = [1, 0, 0]^T. \tag{25}$$

Here we have chosen $\boldsymbol{\xi}^{\mathrm{F}}$ to be real. The most general form of this state is obtained by applying an arbitrary gauge transformation $e^{i\chi_0}$ and a spin rotation about the z-spin axis (i.e. $e^{-i\mathrm{F}_z\chi_1}$) to $\boldsymbol{\xi}^{\mathrm{F}}$. Because the F phase is axially symmetric these transformations leave the properties of the condensate, and its fluctuations, unchanged. The nematic tensor [see Eq. (8)] for $\boldsymbol{\xi}^{\mathrm{F}}$ is

$$q^{\mathrm{F}} = n\begin{pmatrix} \frac{1}{2} & 0 & 0 \\ 0 & \frac{1}{2} & 0 \\ 0 & 0 & 1 \end{pmatrix}. \tag{26}$$

An example of the excitation spectrum for the F state [12] is shown in Fig. 2. This spectrum has phonon (index $\nu = 0$), magnon (index $\nu = 1$), and transverse magnon (index $\nu = 2$) branches.[4] The phonon mode is the Nambu-Goldstone mode for this phase and resides entirely in the $m_F = 1$ component. The phonon is magnetic field independent and corresponds identically to the phonon mode of a scalar gas, but with an effective interaction of $c_0 + c_1 = 4\pi a_2\hbar^2/M$ corresponding to the scattering length of the spin-2 channel.

The magnon modes have energy gaps

$$E^{\mathrm{F}}_{\mathrm{g},1} = 2p - 2c_1n, \tag{27}$$
$$E^{\mathrm{F}}_{\mathrm{g},2} = p - q, \tag{28}$$

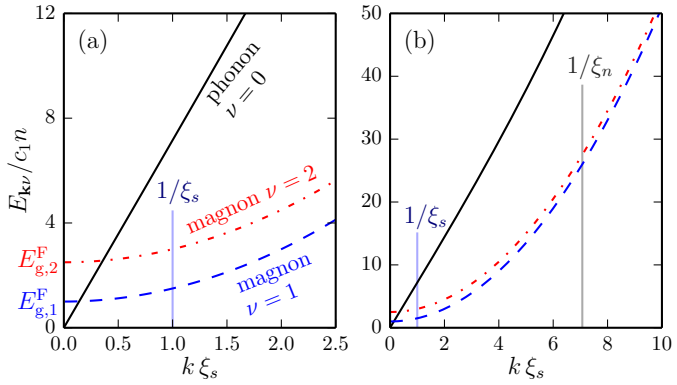

Figure 2. (Color online) Bogoliubov dispersion relations in the F phase. Subplots (a) and (b) focus on different ranges of k values. We show the phonon (solid black line), magnon (dashed blue line), and transverse magnon (dash-dotted red line) branches of the excitation spectra, and attribute these the indices $\nu = 0, 1, 2$, respectively. Parameters: $p = 1.5\,c_1n$, $q = -c_1n$, $c_0 = 50\,c_1$, $c_1 > 0$.

[3] The healing lengths characterize the sizes of spatial structures comparable to the relevant interaction energy, e.g. $\hbar^2/M\xi_s^2 = |c_1|n$.

[4] We identify the phonon branch as that making the largest contribution to the density fluctuations. For the case where the condensate has an average spin we denote the magnon modes as transverse or axial if they give rise to fluctuations that are solely transverse or solely axial to the mean spin, respectively (c.f. [38]).

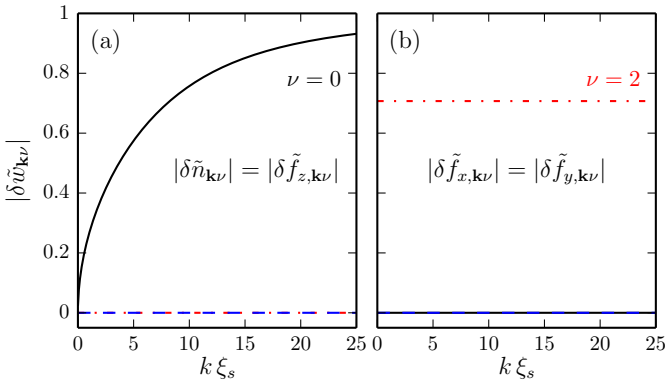

Figure 3. (Color online) Fluctuation amplitudes for the F phase. Subplots (a) $\delta\tilde{n}_{\mathbf{k}\nu}$, $\delta\tilde{f}_{z,\mathbf{k}\nu}$ and (b) $\delta\tilde{f}_{x,\mathbf{k}\nu}$, $\delta\tilde{f}_{y,\mathbf{k}\nu}$, as defined in Eq. (20). The modes (index ν) have the same line types as in Fig. 2. Other parameters as in Fig. 2.

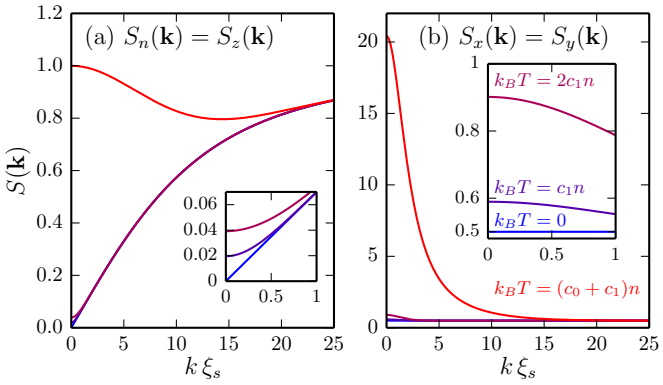

Figure 4. (Color online) Static structure factors for the F phase at various temperatures. Structure factors (a) S_n and S_z (which are identical) and (b) S_x and S_y (which are also identical), as defined in Eq. (21). For temperatures of (from bottom to top curves) $T = \{0, c_1, 2c_1, c_0 + c_1\} \times n/k_B$, as labelled in the inset to (b). Insets reveal additional detail for the lower temperature results at small $k\xi_s$. Other parameters as in Fig. 2.

for $\nu = 1$ and 2, respectively. These branches have quadratic dispersions and are magnetic field sensitive (e.g. revealed by the dependence of $E^{\rm F}_{{\rm g},1}$ and $E^{\rm F}_{{\rm g},2}$ on p and q).

We now consider how these modes relate to fluctuations in the system for the observables of interest. This is most easily seen by examining the fluctuation amplitudes (i.e. $\delta\tilde{w}_{\mathbf{k}\nu}$), which reveal the contributions from the various excitation branches. By summing over these according to Eq. (21), the relevant static structure factors are then computed.

2. *Fluctuations in n and f_z*

Because the condensate resides entirely in the $m_F = 1$ level we trivially have $\mathrm{F}_z\boldsymbol{\xi}^{\rm F} = \mathbb{1}\boldsymbol{\xi}^{\rm F}$ so that [from Eq. (20)] the fluctuation amplitudes $\delta\tilde{n}_{\mathbf{k}\nu}$ and $\delta\tilde{f}_{z,\mathbf{k}\nu}$ are identical.[5] The results in Fig. 3(a) demonstrate that fluctuations in these quantities are entirely due to the phonon mode, with no contribution from either of the magnon modes.

The (identical) static structure factors for density and axial spin are shown in Fig. 4(a) for several temperatures, with analytic limiting results given in Table II. This behavior is similar to that of the density static structure factor for a scalar Bose gas, with the phonon speed of sound set by the scattering length of the spin-2 channel ($c_0 + c_1$). For example, $S_n(\mathbf{0}) = k_BT/[(c_0 + c_1)n]$, and the uncorrelated limit $[S_n(\mathbf{k}) \to 1]$ occurs for wavevectors $k \gg 1/\xi_n$ at sufficiently low temperatures (also see Table II).

3. *Fluctuations in f_x and f_y*

The symmetry of the F phase about the spin z axis is reflected in the identical fluctuations of f_x and f_y. Only the transverse magnon mode contributes to the fluctuation amplitudes $\delta\tilde{f}_{x,y}$, as shown in Fig. 3(b). Because this mode is single particle like (i.e. $\mathbf{u}^T_{\mathbf{k}2} = [0, 1, 0]$, $\mathbf{v}^T_{\mathbf{k}2} = \mathbf{0}$), the fluctuation amplitudes are constant valued with $|\delta\tilde{f}_{x,\mathbf{k}2}| = |\delta\tilde{f}_{x,\mathbf{k}2}| = 1/\sqrt{2}$. Note that the $\nu = 1$ magnon mode is of the form $\mathbf{u}^T_{\mathbf{k}1} = [0, 0, 1]$, $\mathbf{v}^T_{\mathbf{k}1} = \mathbf{0}$, and does not contribute to total density or spin density fluctuations.

The associated structure factors, S_x and S_y, are shown in Fig. 4(b), with analytic limiting results given in Table II. These factors have a non-zero value for $k \to 0$ at $T = 0$, i.e. $S^{T=0}_{x,y}(k \to 0) \neq 0$. This behaviour was also found for a two-component system in Ref. [24], where the magnon mode was also energetically gapped. The energy gap of the transverse magnon mode delays the onset of thermal fluctuations to temperatures $T \gtrsim E^{\rm F}_{{\rm g},2}/k_B$.

B. P phase

1. *Condensate and excitation spectrum*

The P phase occurs for both $c_1 > 0$ and $c_1 < 0$ [see Figs. 1(a),(b)]. In this phase the condensate is unmagnetized and occupies the $m_F = 0$ level, with normalised spinor

$$\boldsymbol{\xi}^{\rm P} = [0, 1, 0]^T. \tag{29}$$

The nematic tensor [see Eq. (8)] for $\boldsymbol{\xi}^{\rm P}$ is

$$q^{\rm P} = n \begin{pmatrix} 1 & 0 & 0 \\ 0 & 1 & 0 \\ 0 & 0 & 0 \end{pmatrix}. \tag{30}$$

The most general form of the P-phase spinor is obtained by applying an arbitrary gauge transformation and a spin rotation about the z-spin axis to $\boldsymbol{\xi}^{\rm P}$. Because the P phase is axially

[5] Note that for the F phase with the condensate in the $m_F = -1$ state, which we denote as $\boldsymbol{\xi}'_F$, then $\mathrm{F}_z\boldsymbol{\xi}^{\rm F'} = -\mathbb{1}\boldsymbol{\xi}^{\rm F'}$.

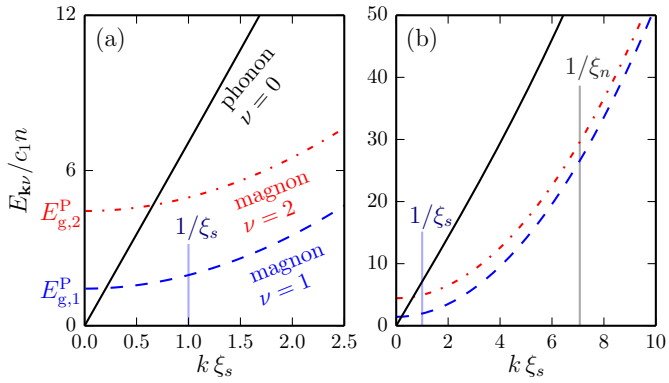

Figure 5. (Color online) Bogoliubov dispersion relations in the P phase. Subplots (a) and (b) focus on different ranges of k values. We show the branches of the excitation spectra for the phonon mode (solid black line) and the two magnon modes (dashed blue line and dash-dotted red line). Parameters: $q = 2.1\,c_1 n$, $c_0 = 50\,c_1$ and $p = 1.5\,c_1 n$, $c_1 > 0$.

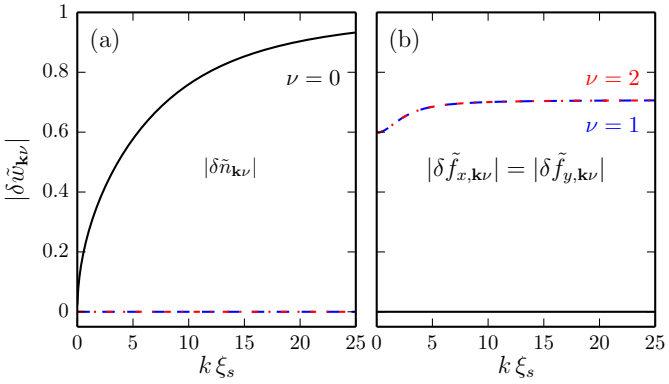

Figure 6. (Color online) Fluctuation amplitudes for the P phase. Subplots (a) $\delta\tilde{n}_{\mathbf{k}\nu}$, and (b) $\delta\tilde{f}_{x,\mathbf{k}\nu}$, $\delta\tilde{f}_{y,\mathbf{k}\nu}$, as defined in Eq. (20). Note $\delta\tilde{f}_{z,\mathbf{k}\nu} = 0$. The modes (index ν) have the same line types as in Fig. 5. Other parameters as in Fig. 5.

symmetric these transformations leave the properties of the condensate, and its fluctuations, unchanged.

An example of the excitation spectrum for the P state [12] is shown in Fig. 5. This spectrum is similar to the F phase [Fig. 2] in that it has a phonon (index $\nu = 0$) and two gapped magnon branches (indices $\nu = 1, 2$). The magnon gaps depend on the magnetic field and are given by

$$E^{\rm P}_{{\rm g},1} = \sqrt{q(q + 2c_1 n)} - p, \tag{31}$$

$$E^{\rm P}_{{\rm g},2} = \sqrt{q(q + 2c_1 n)} + p, \tag{32}$$

for $\nu = 1$ and 2, respectively. The $\nu = 1$ magnon mode is of the form $\mathbf{u}^T_{\mathbf{k}1} = [u, 0, 0]$, $\mathbf{v}^T_{\mathbf{k}1} = [0, 0, v]$, while the $\nu = 2$ magnon mode has $\mathbf{u}^T_{\mathbf{k}2} = [0, 0, u]$, $\mathbf{v}^T_{\mathbf{k}2} = [v, 0, 0]$. The phonon mode resides entirely in the $m_F = 0$ component and corresponds identically to that of a scalar gas with an effective interaction of c_0.

2. *Fluctuations in n and f_z*

Because the condensate resides entirely in the $m_F = 0$ level we have that the f_z fluctuations are identically zero [from Eq. (20)] to the level of approximation we work at here, with the leading order term coming from the small terms we neglected in Eq. (19). We do not consider a higher order treatment here, and take the f_z fluctuations to be zero.

The density fluctuations are entirely due to the phonon mode, which resides in $m_F = 0$, with no contribution from either of the magnon modes [see Fig. 6(a)] . The associated static structure factor is shown in Fig. 7(a) for several temperatures, with analytic limiting results given in Table II.

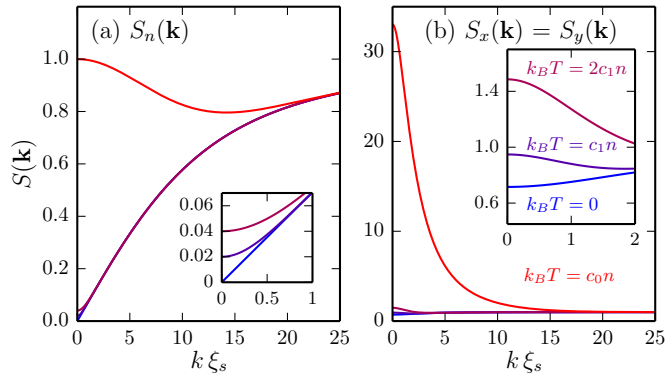

Figure 7. (Color online) Static structure factors for the P phase at various temperatures. Structure factors (a) S_n and (b) S_x, S_y, as defined in Eq. (21). Note $S_z = 0$. For temperatures of (from bottom to top curves) $T = \{0, c_1, 2c_1, c_0\} \times n/k_B$, as labelled in the inset to (b). Insets reveal additional detail for small $k\xi_s$. Other parameters as in Fig. 5.

3. *Fluctuations in f_x and f_y*

Because the P phase is axisymmetric, the f_x and f_y fluctuations are identical, and relevant fluctuation amplitudes are shown in Fig. 6(b). These results show that both magnon modes contribute equally. The associated structure factors are shown in Fig. 7(b), with analytic limiting results given in Table II. Similarly to the S_x and S_y structure factors considered for the F phase, these are also gapped at $k \to 0$ and at zero temperature.

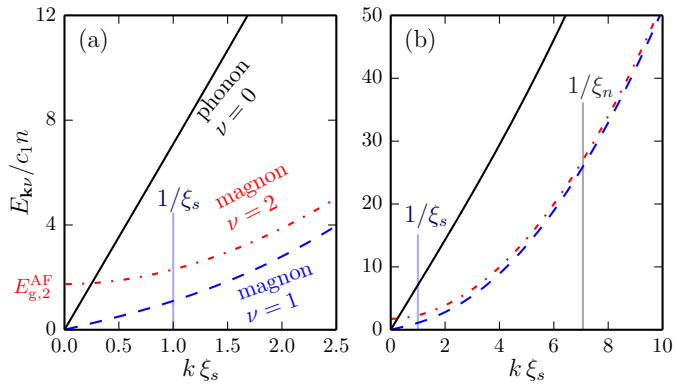

Figure 8. (Color online) Bogoliubov dispersion relations in the AF phase. Subplots (a) and (b) focus on different ranges of k values. We show the phonon (solid black line), axial magnon (dashed blue line), and transverse magnon (dash-dotted red line) branches of the excitation spectra and attribute these the indices $\nu = 0, 1, 2$, respectively. Parameters: $q = -c_1 n$, $c_0 = 50\,c_1$, and $p = 0.2\,c_1 n$, giving $f_z = 0.2\,n$, $\alpha_z \approx 0.98$.

C. AF phase

1. *Condensate and excitation spectrum*

The AF phase occurs only for $c_1 > 0$ [see Fig. 1(a)]. In this phase the condensate takes the form

$$\boldsymbol{\xi}^{\rm AF} = \left[\sqrt{\tfrac{1}{2}(1+f_z/n)}, 0, \sqrt{\tfrac{1}{2}(1-f_z/n)}\right]^T, \qquad (33)$$

and has a z-component of magnetization given by $f_z = p/c_1$ for $|p| \leq c_1 n$. The AF state breaks symmetry about the z axis, as can be seen from its nematic tensor [see Eq. (8)],

$$q^{\rm AF} = n \begin{pmatrix} \frac{1}{2}(1+\alpha_z) & 0 & 0 \\ 0 & \frac{1}{2}(1-\alpha_z) & 0 \\ 0 & 0 & 1 \end{pmatrix}, \qquad (34)$$

where we have introduced the variable

$$\alpha_z = \sqrt{1-(f_z/n)^2}. \qquad (35)$$

We note that $q^{\rm AF}$ corresponds to $q^{\rm F}$ (26) in the limit of a fully magnetized AF state (i.e. $f_z \to n$). The most general form of the AF phase spinor is obtained by applying an arbitrary gauge transformation and a spin rotation about the z-spin axis to $\boldsymbol{\xi}^{\rm AF}$. We note that the spin rotation changes the orientation of the nematic distortion in the spin-xy plane.

An example of the AF excitation spectrum [12] is shown in Fig. 8. It has phonon (index $\nu = 0$), axial magnon (index $\nu = 1$), and transverse magnon (index $\nu = 2$) branches. The AF phase has two broken continuous symmetries giving rise to two Nambu-Goldstone modes: in addition to the phonon mode arising from the broken $U(1)$ symmetry of the condensate, the broken axial spin symmetry (revealed by the nematic tensor) yields a massless axial magnon mode. The axial magnon dispersion mode crosses over from having a linear

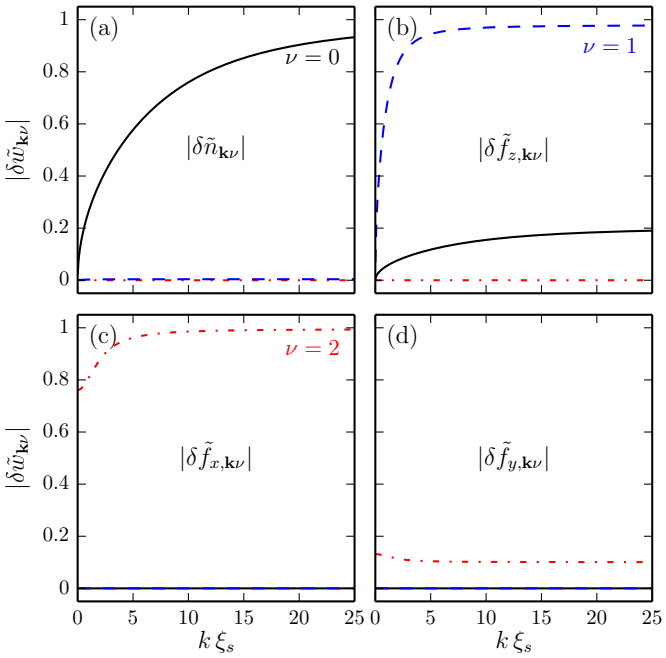

Figure 9. (Color online) Fluctuation amplitudes for the AF phase. Subplots (a) $\delta\tilde{n}_{\mathbf{k}\nu}$, (b) $\delta\tilde{f}_{z,\mathbf{k}\nu}$, (c) $\delta\tilde{f}_{x,\mathbf{k}\nu}$, and (d) $\delta\tilde{f}_{y,\mathbf{k}\nu}$, as defined in Eq. (20). The modes (index ν) have the same line types as in Fig. 8. Other parameters as in Fig. 8.

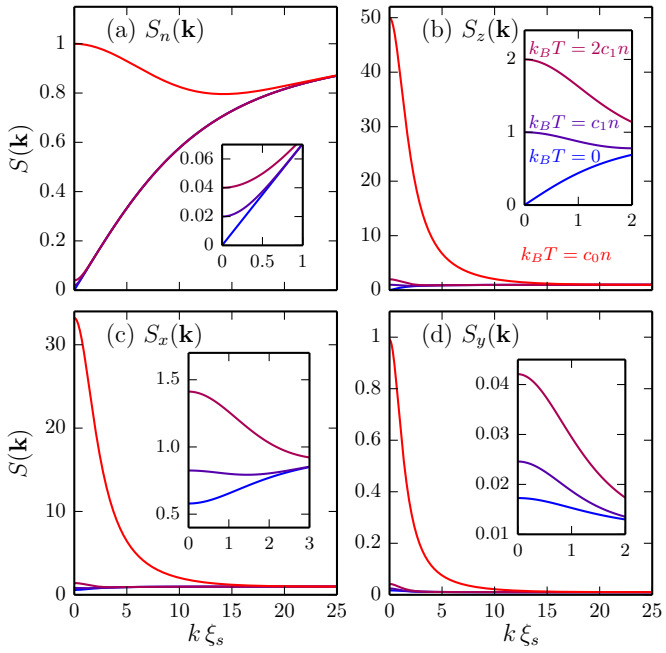

Figure 10. (Color online) Static structure factors for the AF phase at various temperatures. Structure factors (a) S_n, (b) S_z, (c) S_x, and (d) S_y, as defined in Eq. (21). For temperatures of (from bottom to top curves) $T = \{0, c_1, 2c_1, c_0\} \times n/k_B$, as labelled in the inset to (b). Insets reveal the lower temperature results at small $k\xi_s$. Other parameters as in Fig. 8.

to quadratic dependence on k at a wavevector of $k \sim 1/\xi_s$, whereas the phonon mode crosses over at $k \sim 1/\xi_n$. The transverse magnon mode has an energy gap of

$$E_{\mathrm{g},2}^{\mathrm{AF}} = c_1 n \sqrt{(1 - q/c_1 n)^2 - \alpha_z^2}. \tag{36}$$

2. Fluctuations in n

The density fluctuation amplitudes $\delta\tilde{n}_{\mathbf{k}\nu}$ are shown in Fig. 9(a). These results demonstrate that the density fluctuations are dominated by the phonon mode, although a weak contribution arises from the axial magnon mode. This magnon contribution increases as c_1 increases relative to c_0 and also depends on the axial magnetization f_z. (Note: The axial magnon and phonon modes decouple for $f_z = 0$, and at this point the magnon mode does not contribute to $\delta\tilde{n}_{\mathbf{k}\nu}$.)

The density static structure factor (S_n) is shown in Fig. 10(a) for several temperatures. This behavior is similar to that of the density static structure factor in the F phase, except that the phonon speed of sound varies between the value set by $c_0 n$ and $(c_0 + c_1)n$, depending on f_z.

3. Fluctuations in f_z

The axial spin fluctuation amplitudes $\delta\tilde{f}_{z,\mathbf{k}\nu}$ are shown in Fig. 9(b), and demonstrate a dominant contribution from the axial magnon mode, and a smaller, but appreciable contribution from the phonon mode. The associated static structure factor (S_z) is shown in Fig. 10(b). The general behavior is similar to the density fluctuation case, but with the much smaller spin-dependent energy $c_1 n$ being the appropriate energy scale. Thus the fluctuations are more easily thermally activated and the uncorrelated limit [$S_z(\mathbf{k}) \to 1$] is reached at lower wave vectors $k \gg 1/\xi_s$ [also see Table II].

4. Fluctuations in f_x and f_y

The transverse spin fluctuation amplitudes, i.e. $\delta\tilde{f}_{x,\mathbf{k}\nu}$ and $\delta\tilde{f}_{y,\mathbf{k}\nu}$, are shown in Figs. 9(c) and (d), respectively. Only the transverse magnon mode contributes to these. The difference in the behavior of $\delta\tilde{f}_{x,\mathbf{k}\nu}$ and $\delta\tilde{f}_{y,\mathbf{k}\nu}$ reveals the broken symmetry of the AF state about the z-spin axis [c.f. Eq. (34)].

The associated structure factors are shown in Figs. 10(c) and (d). Similarly to the S_x and S_y structure factors for the F and P phases, these also have a non-zero value for $k \to 0$ at $T = 0$. The energy gap of the transverse magnon mode delays the onset of thermal fluctuations to temperatures $T \gtrsim E_{\mathrm{g},2}^{\mathrm{AF}}/k_B$.

D. BA phase

1. Condensate and excitation spectrum

The BA phase occurs for $c_1 < 0$ [see Fig. 1(b)], and in this phase the condensate occupies all three m_F states. The results we present here are for the case of $p = 0$, where the magnetization is purely transverse (i.e. $f_z = 0$). This case has the advantage that it affords a simpler analytic treatment [21, 37], allowing us to write the spinor as

$$\boldsymbol{\xi}^{\mathrm{BA}} = \left[\tfrac{1}{2}\sqrt{1-\tilde{q}}, \sqrt{\tfrac{1}{2}(1+\tilde{q})}, \tfrac{1}{2}\sqrt{1-\tilde{q}}\right]^T, \tag{37}$$

where $\tilde{q} \equiv q/2|c_1|n$. For our choice of a real spinor $\boldsymbol{\xi}^{\mathrm{BA}}$, the magnetization is along the x-spin axis. The most general form of the BA phase spinor is given by an arbitrary gauge transformation and spin rotation about the z-spin axis applied to $\boldsymbol{\xi}^{\mathrm{BA}}$. The nematic tensor for $\boldsymbol{\xi}^{\mathrm{BA}}$ [see Eq. (8)] is

$$q^{\mathrm{BA}} = n \begin{pmatrix} 1 & 0 & 0 \\ 0 & \frac{1}{2}(1+\tilde{q}) & 0 \\ 0 & 0 & \frac{1}{2}(1-\tilde{q}) \end{pmatrix}, \tag{38}$$

which reveals the broken symmetry of the BA state about the z axis due to the transverse magnetization $f_x = \sqrt{1-\tilde{q}^2}$.

The Bogoliubov excitations of the BA phase have been investigated in several recent papers [21, 37] (also see Appendix of [25]).[6] The excitations of the BA phase at $p = 0$ are shown in Fig. 11. Because the BA phase has two broken continuous symmetries, the system has two gapless Nambu-Goldstone modes: a phonon branch (index $\nu = 0$) and a transverse magnon branch (index $\nu = 1$). These two modes are decoupled at $p = 0$. The transverse magnon has the energy dispersion $E_{\mathbf{k}1} = \sqrt{\epsilon_{\mathbf{k}}(\epsilon_{\mathbf{k}} + q)}$ [21], i.e. independent of the interaction parameters, with $\epsilon_{\mathbf{k}} \equiv \hbar^2 k^2/2M$ the free particle energy. Since the quadratic Zeeman sets the relevant energy scale for this magnon, we define an associated length scale $\xi_q \equiv \hbar/\sqrt{Mq}$. The last branch (index $\nu = 2$) is a magnon excitation with energy gap

$$E_{\mathrm{g},2}^{\mathrm{BA}} = 2|c_1|n\sqrt{1-\tilde{q}^2} = 2f_x|c_1|n. \tag{39}$$

This gapped magnon does couple to the phonon branch, and they have an avoided crossing, as revealed in Fig. 11(a) and inset. We have chosen to switch the labelling on either side of this crossing to match the labelling choice made in Ref. [37] and also to ensure that away from the crossing the $\nu = 0$ mode has a phonon character (i.e. a dominant effect on density fluctuations). The coupling between these two modes is small so that the avoided crossing occurs over a narrow range of k vectors, with the energy gap between these branches being

$$\Delta_C = q\sqrt{1-\tilde{q}^2}\sqrt{\frac{|c_1|}{c_0}}, \tag{40}$$

[6] While various analytic results have been reported for the $p = 0$ case [21], the understanding of the $p \neq 0$ case is based largely on numerical results [37].

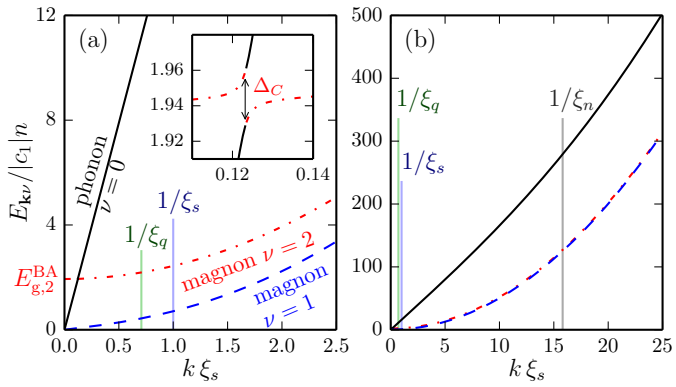

Figure 11. (Color online) Bogoliubov dispersion relations in the BA phase. Subplots (a) and (b) focus on different ranges of k values. We show the branches of the excitation spectra for the phonon mode (solid black line) and the axial (dashed blue line; note the magnetization axis is x) and transverse (dash-dotted red line) magnon modes. Inset to (a) reveals an avoided crossing between the phonon and transverse magnon modes. Parameters: $q = 0.5\,|c_1|n$, $c_0 = -250\,c_1$, $p = 0$ and $c_1 < 0$.

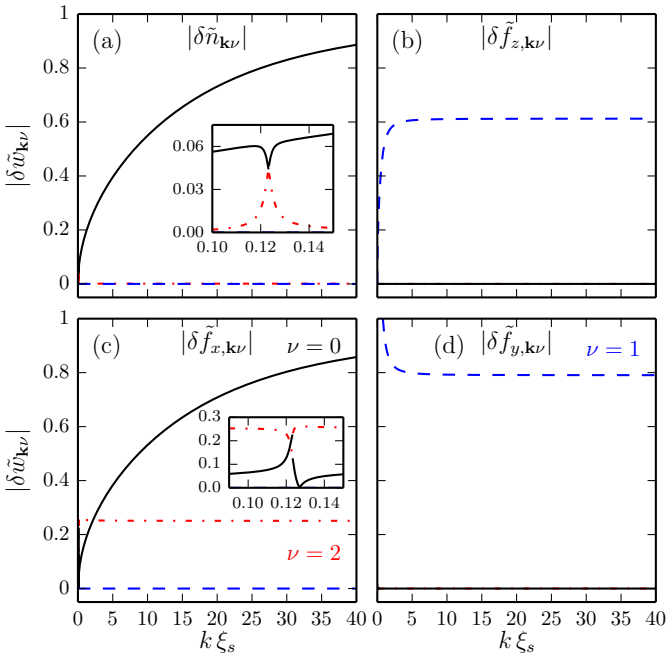

Figure 12. (Color online) Fluctuation amplitudes for the BA phase. Subplots (a) $\delta\tilde{n}_{\mathbf{k}\nu}$, (b) $\delta\tilde{f}_{z,\mathbf{k}\nu}$, (c) $\delta\tilde{f}_{x,\mathbf{k}\nu}$, and (d) $\delta\tilde{f}_{y,\mathbf{k}\nu}$, as defined in Eq. (20). The modes (index ν) have the same line types as in Fig. 11. Insets to (a) and (c) reveal additional detail for $k\xi_s$ close to the avoided crossing. Other parameters as in Fig. 11.

to lowest order in c_1/c_0.

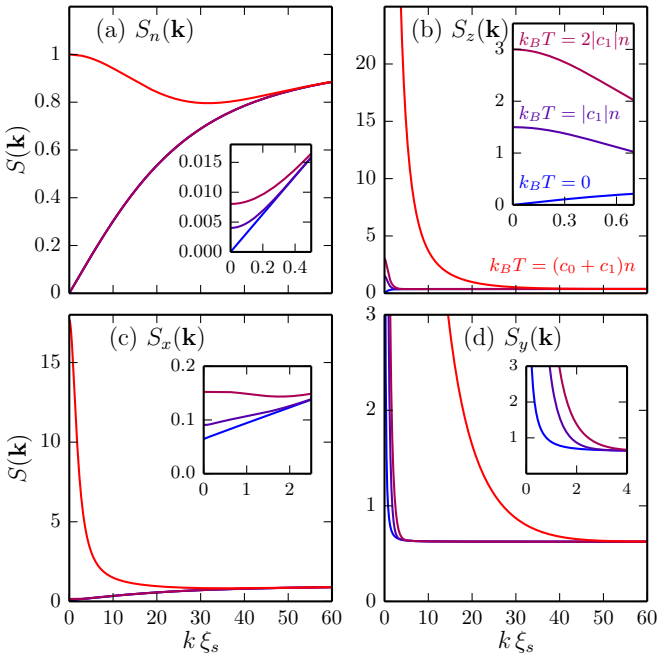

Figure 13. (Color online) Static structure factors for the BA phase at various temperatures. Structure factors (a) S_n, (b) S_z, (c) S_x, and (d) S_y, as defined in Eq. (21). For temperatures of (from bottom to top curves) $T = \{0, |c_1|, 2|c_1|, c_0 + c_1\}\times n/k_B$, as labelled in the inset to (b). Insets reveal additional detail for small $k\xi_s$. Other parameters as in Fig. 11.

2. *Fluctuations in n and f_z*

From Fig. 12(a) we see that the dominant contribution to density fluctuations comes from the phonon mode, although a contribution from the (gapped) axial magnon mode occurs near the avoided crossing noted in the spectrum.[7] In contrast, the f_z fluctuations come entirely from the (Nambu-Goldstone) transverse magnon branch ($\nu = 1$) [see Fig. 12(b)].

The structure factors S_n and S_z are shown in Fig. 13(a) and (b), respectively, with analytic expressions for the limiting behavior provided in Table II. Interestingly, the long wavelength fluctuations of the z component of magnetization is set by the quadratic Zeeman energy, i.e. $S_z(0) = (1-\tilde{q})k_BT/q$. This diverges for $q \to 0$ as the full spin rotational symmetry [$SO(3)$] is restored (noting that we have set $p = 0$).

3. *Fluctuations in f_x and f_y*

Because the magnetization lies along x for our choice of p and $\boldsymbol{\xi}^{\rm BA}$, fluctuations in f_x correspond to fluctuations in

[7] The rapid variation in $\{\delta\tilde{n}_{\mathbf{k}0}, \delta\tilde{n}_{\mathbf{k}2}\}$ and $\{\delta\tilde{f}_{x,\mathbf{k}0}, \delta\tilde{f}_{x,\mathbf{k}2}\}$ for $k \approx 0.12/\xi_s$ occurs because the phonon and transverse magnon hybridize near the anti-crossing. We emphasise that the summed contribution of these fluctuations to the relevant structure factors is smooth.

Phase	Observable(s)	$S_w(k\to 0)$		$S_w(k\to\infty)$
		$T=0$	$T>0$	
F	n, f_z	$\sqrt{\frac{\epsilon_{\mathbf{k}}}{2(c_0+c_1)n}}$	$\frac{k_BT}{(c_0+c_1)n}$	1
	f_x, f_y	$\frac{1}{2}\coth\left(\frac{E^{\rm F}_{{\rm g},2}}{2k_BT}\right)$		$\frac{1}{2}$
P	n	$\frac{k\xi_n}{2}$	$\frac{k_BT}{c_0n}$	1
	f_z	0		0
	f_x, f_y	$\frac{\coth\left(\frac{E^{\rm P}_{{\rm g},1}}{2k_BT}\right)+\coth\left(\frac{E^{\rm P}_{{\rm g},2}}{2k_BT}\right)}{2\sqrt{1+2c_1n/q}}$		1
AF	n	$\left[1+\frac{f_z^2}{n^2}\left(-\frac{1}{2}\frac{c_1}{c_0}+\sqrt{1-\frac{f_z^2}{n^2}\frac{c_1^{3/2}}{c_0^{3/2}}}\right)\right]\frac{k\xi_n}{2}$	$\frac{k_BT}{c_0n}$	1
	f_z	$\left[\sqrt{1-\frac{f_z^2}{n^2}\left(1-\frac{3f_z^2}{2n^2}\frac{c_1}{c_0}\right)}+\frac{f_z^2}{n^2}\sqrt{\frac{c_1}{c_0}}\right]\frac{k\xi_s}{2}$	$\frac{k_BT}{c_1n}$	1
	$\substack{f_x\to+\\ f_y\to-}$	$\frac{1}{2}\left(\frac{1\pm\alpha_z}{1\pm\alpha_z-q/c_1n}\right)\frac{E^{\rm AF}_{{\rm g},2}}{c_1n}\coth\left(\frac{E^{\rm AF}_{{\rm g},2}}{2k_BT}\right)$		$\frac{1}{2}(1\pm\alpha_z)$
BA	n	$\sqrt{\frac{\epsilon_{\mathbf{k}}}{2(c_0+c_1)n}}$	$\frac{k_BT}{(c_0+c_1)n}$	1
$(p=0)$	f_x	$\frac{\tilde{q}^2}{\sqrt{1-\tilde{q}^2}}+\frac{1}{1-\tilde{q}^2}\sqrt{\frac{\epsilon_{\mathbf{k}}}{2(c_0+c_1)n}}$	$\frac{k_BT}{(c_0+c_1)n}\frac{1}{1-\tilde{q}^2}+\frac{\tilde{q}^2}{\sqrt{1-\tilde{q}^2}}\coth\left(\frac{E^{\rm BA}_{{\rm g},2}}{2k_BT}\right)$	1
	f_y	$\frac{1}{2}(1+\tilde{q})\sqrt{\frac{q}{\epsilon_{\mathbf{k}}}}$	$(1+\tilde{q})\frac{k_BT}{\epsilon_{\mathbf{k}}}$	$\frac{1}{2}(1+\tilde{q})$
	f_z	$\frac{1}{2}(1-\tilde{q})\sqrt{\frac{\epsilon_{\mathbf{k}}}{q}}$	$(1-\tilde{q})\frac{k_BT}{q}$	$\frac{1}{2}(1-\tilde{q})$

Table II. Large and small k limits of the structure factors. Where necessary in the $k\to 0$ limits we distinguish between $T=0$ and $T>0$ results: In the $T=0$ case we give a k expansion, whereas for $T>0$ we give the structure factor value at $k=0$. For n and f_z in the AF phase, the $T=0$ results are the first terms in an expansion for $c_1\ll c_0$ and the finite T results are valid for $|f_z|<n$.

the length of the magnetization. Fig. 12(c) reveals that both the gapped magnon mode and the phonon mode contribute to these fluctuations. In contrast, fluctuations in f_y are orthogonal to the direction of magnetization and act to restore the axial symmetry [$SO(2)$] of the Hamiltonian. In Fig. 12(d) we see that these fluctuations are entirely due to the (Nambu-Goldstone) transverse magnon mode, and that these fluctuations diverge as $k\to 0$. The divergence is clearly apparent in S_y [see Fig. 13(d)] and is seen to go as k^{-2} for small k at finite temperature [see Table II].

4. *BA phase for $p\neq 0$*

We conclude by briefly commenting on the qualitative behavior for $p\neq 0$. In this case the condensate magnetization tilts out of the xy-plane and the Nambu-Goldstone branches (i.e. $\nu=0$ and $\nu=1$ branches) become coupled (c.f. at $p=0$, where the only coupling is between the $\nu=0$ and $\nu=2$ branches, giving rise to the avoided crossing). In Ref. [37] this occurrence was referred to as phonon-magnon coupling. As a result of this coupling the $\nu=1$ mode contributes to density fluctuations, and the $\nu=0$ mode contributes to f_z fluctuations.

V. DISCUSSION AND CONCLUSIONS

In this paper we have developed a formalism for the static structure factor of a uniform spin-1 condensate subject to constant linear and quadratic Zeeman shifts. Our results are based on the Bogoliubov formalism and are accurate to the leading order term proportional to the condensate density. The static structure factors are an important tool in quantifying fluctuations for scalar and binary systems (e.g. see [39–42]), and this work is important for extending such results to the spinor system.

A feature of spinor condensates is that additional continuous symmetries can be broken, leading to new Nambu-Goldstone modes, as is predicted to occur for the AF and BA phases. For the AF phase we found that the asymmetry in the nematic order of the condensate was revealed through the f_x

Phase	Observable(s)	$\lvert\delta\hat{w}_{\mathbf{k}\nu}\rvert^2$		
		$\nu=0$	$\nu=1$	$\nu=2$
F	n, f_z	$\sqrt{\frac{\epsilon_{\mathbf{k}}}{2(c_0+c_1)n}}$	0	0
	f_x, f_y	0	0	$\frac{1}{2}$
P	n	$\frac{k\xi_n}{2}$	0	0
	f_z	0	0	0
	f_x, f_y	0	$\frac{1}{2\sqrt{1+2c_1n/q}}$	$\frac{1}{2\sqrt{1+2c_1n/q}}$
AF	n	$\left(1-\frac{1}{2}\frac{f_z^2}{n^2}\frac{c_1}{c_0}\right)\frac{k\xi_n}{2}$	$\frac{f_z^2}{n^2}\sqrt{1-\frac{f_z^2}{n^2}\frac{c_1^{3/2}}{c_0^{3/2}}}\frac{k\xi_n}{2}$	0
	f_z	$\frac{f_z^2}{n^2}\sqrt{\frac{c_1}{c_0}}\frac{k\xi_s}{2}$	$\sqrt{1-\frac{f_z^2}{n^2}}\left(1-\frac{3f_z^2}{2n^2}\frac{c_1}{c_0}\right)\frac{k\xi_s}{2}$	0
	$\substack{f_x\to+\\f_y\to-}$	0	0	$\frac{1}{2}\left(\frac{1\pm\alpha_z}{1\pm\alpha_z-q/c_1n}\right)\frac{E^{\mathrm{AF}}_{\mathrm{g},2}}{c_1n}$
BA	n	$\sqrt{\frac{\epsilon_{\mathbf{k}}}{2(c_0+c_1)n}}$	0	$\frac{\tilde{q}^2}{(1-\tilde{q}^2)^{3/2}}\left(\frac{\epsilon_{\mathbf{k}}}{c_1n}\right)^2$
$(p=0)$	f_x	$\frac{1}{1-\tilde{q}^2}\sqrt{\frac{\epsilon_{\mathbf{k}}}{2(c_0+c_1)n}}$	0	$\frac{\tilde{q}^2}{\sqrt{1-\tilde{q}^2}}$
	f_y	0	$\frac{1}{2}(1+\tilde{q})\sqrt{\frac{q}{\epsilon_{\mathbf{k}}}}$	0
	f_z	0	$\frac{1}{2}(1-\tilde{q})\sqrt{\frac{\epsilon_{\mathbf{k}}}{q}}$	0

Table III. Small k limits of fluctuation amplitudes. For n and f_z in the AF phase, the results are the first terms in an expansion for $c_1 \ll c_0$. Where the entry is zero, the fluctuation amplitude is zero for all k.

and f_y fluctuations. In the BA phase we observed a divergence in the f_y fluctuations associated with the spontaneous development of a transverse (axial-symmetry-breaking) magnetization. Our results show that this divergence arises from the Nambu-Goldstone magnon mode. Interestingly, such a divergence in fluctuations was not observed in our results for the AF phase, which also has a Nambu-Goldstone magnon branch. The reason is that for the AF phase the broken symmetry manifests only in the nematic order of the condensate, not in the spin order. Indeed, an immediate extension of our theory is to assess fluctuations of the nematic density,

$$\hat{q}_{\alpha\beta}(\mathbf{x}) = \hat{\boldsymbol{\psi}}^{\dagger}(\mathbf{x})\mathrm{Q}_{\alpha\beta}\hat{\boldsymbol{\psi}}(\mathbf{x}), \tag{41}$$

as a generalisation of Eq. (8). We find that for the AF state the fluctuations in q_{xy} diverge for $k \to 0$ due to both Nambu-Goldstone modes, with the magnon branch dominating. Because some of the techniques used to image the spin density are also sensitive to the nematic density (e.g. see [13]), the measurement of such fluctuations may also be possible in experiments.

Our analysis here has been for a uniform system, and several factors will become important in applying these results to the experimental regime. First, external trapping potentials cause the total density of the condensate to vary spatially and a full treatment of the trapped system would require a large-scale numerical solution of the Gross-Pitaevskii equation for the condensate and of the Bogoliubov-de Gennes equations for the quasiparticles. However, our analysis can be applied to this situation using the local density approximation, i.e. we consider the gas to be homogeneous at each point in space using the local value of the condensate density. A discussion of the local density approximation in relation to the density response of a scalar condensate is presented in Ref. [22]. Second, in our analysis of the AF and BA phases we have assumed that the axisymmetry is broken uniformly over the entire system. For the case where the system forms domains of local broken axisymmetry our analysis will only apply to each domain (also see discussion in [37]).

ACKNOWLEDGMENTS

We thank Y. Kawaguchi for providing feedback on the manuscript. We acknowledge support by the Marsden Fund of New Zealand (contract UOO1220).

Appendix A: Limits of quasiparticle amplitudes

The large k limits of the structure factors can be found directly from Eq. (23). For the small k limits, we diagonalise a 6×6 matrix to give the quasiparticle amplitudes for each phase. For the F and P phases, the quasiparticle amplitudes are given in Sec. 5.2 of [12], and for the BA phase they are given in [21]. For the AF phase, the quasiparticle amplitudes of the gapped mode are given in [12]. The two ungapped modes have $[\mathbf{u}_{\mathbf{k}\nu}]_0 = [\mathbf{v}_{\mathbf{k}\nu}]_0 = 0$ (where $[\mathbf{q}]_m$ is the m component of the vector $\mathbf{q}$), so since $[\boldsymbol{\xi}^{\rm AF}]_0 = 0$, $\delta\hat{f}_{x,\mathbf{k}\nu} = \delta\hat{f}_{y,\mathbf{k}\nu} = 0$ for these two modes. For $\hat{n}$ and $\hat{f}_z$, we need the differences (for $0 < c_1 \ll c_0$)

$$[\mathbf{u}_{\mathbf{k}0} - \mathbf{v}_{\mathbf{k}0}]_\pm = \sqrt{1 \pm \frac{f_z}{n}} \left[1 \pm \frac{f_z}{n}\left(1 \mp \frac{5f_z}{4n}\right)\frac{c_1}{c_0}\right] \frac{\sqrt{k\xi_n}}{2}, \tag{A1}$$

$$[\mathbf{u}_{\mathbf{k}1} - \mathbf{v}_{\mathbf{k}1}]_\pm = \frac{\sqrt{1 \mp \frac{f_z}{n}}}{(1 - \frac{f_z^2}{n^2})^{1/4}} \left[\pm 1 - \frac{f_z}{n}\left(1 \pm \frac{3f_z}{4n}\right)\frac{c_1}{c_0}\right] \frac{\sqrt{k\xi_s}}{2}, \tag{A2}$$

which reduce to the result in [12] for $f_z = 0$ and small k. We use Eq. (20) to obtain the fluctuation amplitudes from the quasiparticle amplitudes, with results shown in Table III. To get the small k limits of the structure factors from the quasiparticle amplitudes, we use Eq. (21).

[1] T.-L. Ho, Phys. Rev. Lett. **81**, 742 (1998).
[2] T. Ohmi and K. Machida, J. Phys. Soc. Jpn **67**, 1822 (1998).
[3] J. Stenger, S. Inouye, D. M. Stamper-Kurn, H.-J. Miesner, A. P. Chikkatur, and W. Ketterle, Nature **396**, 345 (1998).
[4] M.-S. Chang, C. D. Hamley, M. D. Barrett, J. A. Sauer, K. M. Fortier, W. Zhang, L. You, and M. S. Chapman, Phys. Rev. Lett. **92**, 140403 (2004).
[5] M.-S. Chang, Q. Qin, W. Zhang, L. You, and M. S. Chapman, Nat. Phys. **99**, 111 (2005).
[6] A. T. Black, E. Gomez, L. D. Turner, S. Jung, and P. D. Lett, Phys. Rev. Lett. **99**, 070403 (2007).
[7] M. Vengalattore, S. R. Leslie, J. Guzman, and D. M. Stamper-Kurn, Phys. Rev. Lett. **100**, 170403 (2008).
[8] M. Vengalattore, J. Guzman, S. R. Leslie, F. Serwane, and D. M. Stamper-Kurn, Phys. Rev. A **81**, 053612 (2010).
[9] Y. Liu, E. Gomez, S. E. Maxwell, L. D. Turner, E. Tiesinga, and P. D. Lett, Phys. Rev. Lett. **102**, 225301 (2009).
[10] L. E. Sadler, J. M. Higbie, S. R. Leslie, M. Vengalattore, and D. M. Stamper-Kurn, Nature **443**, 312 (2006).
[11] Y. Liu, S. Jung, S. E. Maxwell, L. D. Turner, E. Tiesinga, and P. D. Lett, Phys. Rev. Lett. **102**, 125301 (2009).
[12] Y. Kawaguchi and M. Ueda, Physics Reports **520**, 253 (2012).
[13] D. M. Stamper-Kurn and M. Ueda, Rev. Mod. Phys. **85**, 1191 (2013).
[14] E. M. Bookjans, C. D. Hamley, and M. S. Chapman, Phys. Rev. Lett. **107**, 210406 (2011).
[15] B. Lücke, M. Scherer, J. Kruse, L. Pezzé, F. Deuretzbacher, P. Hyllus, O. Topic, J. Peise, W. Ertmer, J. Arlt, L. Santos, A. Smerzi, and C. Klempt, Science **334**, 773 (2011).
[16] C. D. Hamley, C. S. Gerving, T. M. Hoang, E. M. Bookjans, and M. S. Chapman, Nature Physics **8**, 305 (2012).
[17] A. Vinit, E. M. Bookjans, C. A. R. Sá de Melo, and C. Raman, Phys. Rev. Lett. **110**, 165301 (2013).
[18] I. Carusotto and E. J. Mueller, Journal of Physics B: Atomic, Molecular and Optical Physics **37**, S115 (2004).
[19] J. M. Higbie, L. E. Sadler, S. Inouye, A. P. Chikkatur, S. R. Leslie, K. L. Moore, V. Savalli, and D. M. Stamper-Kurn, Phys. Rev. Lett. **95**, 050401 (2005).
[20] K. Eckert, L. Zawitkowski, A. Sanpera, M. Lewenstein, and E. S. Polzik, Phys. Rev. Lett. **98**, 100404 (2007).
[21] S. Uchino, M. Kobayashi, and M. Ueda, Phys. Rev. A **81**, 063632 (2010).
[22] F. Zambelli, L. Pitaevskii, D. M. Stamper-Kurn, and S. Stringari, Phys. Rev. A **61**, 063608 (2000).
[23] M.-C. Chung and A. B. Bhattacherjee, Phys. Rev. Lett. **101**, 070402 (2008).
[24] M. Abad and A. Recati, Eur. Phys. J. D **67**, 148 (2013).
[25] R. Barnett, A. Polkovnikov, and M. Vengalattore, Phys. Rev. A **84**, 023606 (2011).
[26] C.-L. Hung, X. Zhang, N. Gemelke, and C. Chin, Nature **470**, 236 (2011).
[27] A. Blumkin, S. Rinott, R. Schley, A. Berkovitz, I. Shammass, and J. Steinhauer, Phys. Rev. Lett. **110**, 265301 (2013).
[28] A. G. Sykes and R. J. Ballagh, Phys. Rev. Lett. **107**, 270403 (2011).
[29] J. Steinhauer, R. Ozeri, N. Katz, and N. Davidson, Phys. Rev. Lett. **88**, 120407 (2002).
[30] E. D. Kuhnle, H. Hu, X.-J. Liu, P. Dyke, M. Mark, P. D. Drummond, P. Hannaford, and C. J. Vale, Phys. Rev. Lett. **105**, 070402 (2010).
[31] S. Hoinka, M. Lingham, M. Delehaye, and C. J. Vale, Phys. Rev. Lett. **109**, 050403 (2012).
[32] C. Sanner, E. J. Su, A. Keshet, W. Huang, J. Gillen, R. Gommers, and W. Ketterle, Phys. Rev. Lett. **106**, 010402 (2011).
[33] J. Guzman, G.-B. Jo, A. N. Wenz, K. W. Murch, C. K. Thomas, and D. M. Stamper-Kurn, Phys. Rev. A **84**, 063625 (2011).
[34] A. Tokuno and S. Uchino, Phys. Rev. A **87**, 061604 (2013).
[35] F. Gerbier, A. Widera, S. Fölling, O. Mandel, and I. Bloch, Phys. Rev. A **73**, 041602 (2006).
[36] E. M. Bookjans, A. Vinit, and C. Raman, Phys. Rev. Lett. **107**, 195306 (2011).
[37] K. Murata, H. Saito, and M. Ueda, Phys. Rev. A **75**, 013607 (2007).
[38] E. Yukawa and M. Ueda, Phys. Rev. A **86**, 063614 (2012).
[39] G. E. Astrakharchik, R. Combescot, and L. P. Pitaevskii, Phys. Rev. A **76**, 063616 (2007).
[40] M. Klawunn, A. Recati, L. P. Pitaevskii, and S. Stringari, Phys. Rev. A **84**, 033612 (2011).
[41] A. Recati and S. Stringari, Phys. Rev. Lett. **106**, 080402 (2011).
[42] R. N. Bisset and P. B. Blakie, Phys. Rev. Lett. **110**, 265302 (2013).